Preclinical Evaluation of a Novel TSPO PET Ligand 2-(7-Butyl-2-(4-(2-[18F]Fluoroethoxy) phenyl)-5-Methylpyrazolo[1,5-*a*]Pyrimidin-3-yl)-*N,N*-Diethylacetamide (18F-VUIIS1018A) to Image Glioma

Dewei Tang[1,2], **Jun Li**[3,4,5], **Michael L. Nickels**[3,4,5], **Gang Huang**[1,2], **Allison S. Cohen**[3,4], **H. Charles Manning**[3,4,5,6,7,8,9]

[1]Center for Molecular Imaging, Shanghai University of Medicine & Health Sciences, Shanghai, China

[2]Department of Nuclear Medicine, Renji Hospital, School of Medicine, Shanghai Jiao Tong University, 160 Pujian Road, Pudong New District, Shanghai, 200127, China

[3]Vanderbilt University Institute of Imaging Science, Vanderbilt University Medical Center, Nashville, TN, USA

[4]Vanderbilt Center for Molecular Probes (CMP), Vanderbilt University Medical School, 1161 21st Ave. S., AA 1105 MCN, Nashville, TN, 37232-2310, USA

[5]Department of Radiology and Radiological Sciences, Vanderbilt University Medical Center, Nashville, TN, USA

[6]Program in Chemical and Physical Biology, Vanderbilt University Medical Center, Nashville, TN, USA

[7]Vanderbilt Ingram Cancer Center, Vanderbilt University Medical Center, Nashville, TN, USA

[8]Department of Biomedical Engineering, Vanderbilt University, Nashville, TN, USA

[9]Department of Neurosurgery, Vanderbilt University Medical Center, Nashville, TN, USA

Abstract

Purpose: There is an urgent need for the development of novel positron emission tomography (PET) tracers for glioma imaging. In this study, we developed a novel PET probe ([^{18}F]VUIIS1018A) by targeting translocator protein (TSPO), an imaging biomarker for glioma. The purpose of this preclinical study was to evaluate this novel TSPO probe for glioma imaging.

Procedures: In this study, we synthesized [^{19}F]VUIIS1018A and the precursor for radiosynthesis of [^{18}F]VUIIS1018A. TSPO binding affinity was confirmed using a radioligand

competitive binding assay in C6 glioma cell lysate. Further, dynamic imaging studies were performed in rats using a microPET system. These studies include displacement and blocking studies for ligand reversibility and specificity evaluation, and compartment modeling of PET data for pharmacokinetic parameter measurement using metabolite-corrected arterial input functions and PMOD.

Results: Compared to previously reported TSPO tracers including [^{18}F]VUIIS1008 and [^{18}F]DPA-714, the novel tracer [^{18}F]VUIIS1018A demonstrated higher binding affinity and BP$_{ND}$. Pretreatment with the cold analog [^{19}F]VUIIS1018A could partially block tumor accumulation of this novel tracer. Further, compartment modeling of this novel tracer also exhibited a greater tumor-to-background ratio, a higher tumor binding potential and a lower brain binding potential when compared with other TSPO probes, such as [^{18}F]DPA-714 and [^{18}F]VUIIS1008.

Conclusions: These studies illustrate that [^{18}F]VUIIS1018A can serve as a promising TSPO PET tracer for glioma imaging and potentially imaging of other solid tumors.

Keywords

TSPO; PET; Molecular imaging; Glioma; VUIIS1018A; DPA-714; Cancer imaging

Introduction

Malignant gliomas are the most common primary brain tumors and are characterized by invasive growth and recalcitrance to therapy. The use of pathology for the diagnosis, grading, and classification of gliomas is confounded by tumor heterogeneity and sampling errors associated with obtaining tissue specimens through biopsy or surgical resection. Hence, imaging is frequently used to support clinical decisions by providing a non-invasive method to characterize the whole tumor and metastases [1]. Though ubiquitously employed clinically, X-ray computed tomography (CT) and magnetic resonance imaging (MRI) provide little molecular information attributable to the pathology of disease and tend to poorly discriminate margins, particularly where tumors are highly infiltrative. As another non-invasive imaging modality, positron emission tomography (PET) imaging overcomes many of the limitations associated with conventional brain tumor imaging modalities and offers unique advantages including improved sensitivity and the ability to differentiate tissues based upon molecular characteristics. Currently, 2-deoxy-2-[^{18}F]fluoro-D-glucose ([^{18}F]FDG) is the most widely used PET tracer for brain tumor imaging in the clinic [2]. However, due to tracer accumulation in normal brain tissues, PET imaging using [^{18}F]FDG can only generate modest to poor tumor-to-background ratios. Thus, there remains a strong unmet clinical need to develop and validate novel molecular imaging ligands for the detection and characterization of gliomas.

Translocator protein (TSPO) is an 18 kDa membrane protein typically localized to the outer mitochondrial membrane. Formerly known as the peripheral benzodiazepine receptor (PBR), TSPO participates in a variety of cellular functions, including steroid biosynthesis, cholesterol metabolism, cell proliferation, and apoptosis. [3]. Accordingly, TSPO expression is elevated in numerous clinically important diseased states, including neuroinflammation

[4–8] and cancer [9–12]. As a hallmark of aggressive tumors, TSPO expression has been linked with disease progression and diminished survival in oncology.

A variety of TSPO ligands have been reported for imaging a number of cancers, including colon cancer [13], breast cancer [14–16], and glioma [17–21]. Since TSPO tends to have elevated expression in brain tumor tissues while maintaining low expression in normal brain, it is ideal to use TSPO PET tracers to visualize and quantify glioma [22]. In our previous studies, *N*-[18F]fluoroacetyl-*N*-(2,5-dimethoxybenzyl)-2-phenoxyaniline ([18F]PBR06) [18] and *N, N*-diethyl-2-(2-(4-(2-[18F]fluoroethoxy)phenyl)-5,7-dimethylpyrazolo[1,5-*a*]pyrimidin-3-yl)acetamide ([18F]DPA-714) [17] have been used for glioma imaging. Further, we reported the synthesis and structure activity relationship (SAR) analysis of a library of novel pyrazolopyrimidines [23], which led to the discovery of a novel ligand 2-(5,7-diethyl-2-(4-(2-fluoroethoxy)phenyl)pyrazolo[1,5-a]pyrimidin-3-yl)-*N,N*-diethylacetamide (VUIIS1008) that exhibited a 36-fold enhancement in binding affinity compared to the previously reported TSPO ligand, DPA-714 [17, 23]. Herein, we further modified the five and seven positions of the pyrazolopyrimidinal scaffold and discovered a novel TSPO ligand VUIIS1018A (Fig. 1), which features a 700-fold and a 20-fold enhancement in binding affinity when compared with DPA-714 and VUIIS1008, respectively [17, 23].

To evaluate its *in vivo* performance in C6-glioma imaging, we prepared the radiolabeled ligand [18F]VUIIS1018A and performed a series of analyses including *in vivo* PET imaging, radiometabolite analysis, and pharmacokinetic modeling.

Materials and Methods

Chemicals

[3H]PK 11195 was purchased from PerkinElmer. Phosphate-buffered saline (PBS) and CytoScint ES Liquid Scintillation Cocktail were purchased from MP biomedicals. 2,4-Octanedione was purchased from Alfa Aesar. All other synthesis reagents were purchased from Sigma-Aldrich Chemical Company and used as supplied.

Ligand and Radioligand Precursor Preparation

As shown in Scheme 1 (see Electronic Supplementary Material: ESM), **2A** and **2B** can be prepared *via* a two-step synthetic route starting from previously reported compound **1** [23, 24]. Compound **1** is combined with octane-2,4-dione to afford the desired pyrimidine ring heterocycle, followed by de-protection of the methyl ether to reveal the phenol moiety *via* reaction with hydrogen bromide, HBr. Further reaction of **2A** and **2B** with the appropriate tosylates produced **3A** (VUIIS1018A), as the cold analog of the F-18 labeled probe, **3B** (VUIIS1018B) and **4A**, as a precursor for the radiosynthesis of the PET tracer [18F]VUIIS1018A. Structure characterization was performed using liquid chromatography-mass spectrometry (LCMS), H-1 and C-13 NMR (see ESM).

In Vitro TSPO-Binding Assay

C6 cells were collected and washed with PBS buffer three times, then frozen and thawed three times in lysis buffer (5.0 mM HEPES, 0.21 M D-mannitol, 0.07 M sucrose, 2.0 mM benzamidine, 2.0 mM toluenesulfonyl fluoride, 4.0 mM $MgCl_2$, pH 7.4) to produce C6 cell lysate (0.5 mg/ml). The obtained C6 cell lysate (0.3 ml) was then incubated with [^{3}H]PK 11195 (final concentration = 0.6 nM) and TSPO ligands (10^{-5} to 10^{-14} M) in a total volume of 1.0 ml for 2 h at 25 °C. The reaction was terminated by rapid filtration through a Brandel harvester (Gaithersburg, MD, USA) and collection onto a filter presoaked with 0.3 % polyethylenimine. Filters were then punched out into scintillation vials and bound radioactivity measured on a Beckman LS 6000 Scintillation Counter (Brea, California, USA). Binding affinity (IC_{50}) was calculated using GraphPad Prism (La Jolla, CA, USA) in triplicates.

Radiosynthesis

Radiosynthesis was carried out by the Center for Molecular Probes Radiochemistry Core (VUMC). [^{18}F]VUIIS1018A was synthesized from the tosylate ester precursor (**4A** in Suppl. Scheme 1, ESM). In brief, using a commercial apparatus (TRACERlab FX$_{F-N}$; GE Healthcare, Little Chalfont, UK), aqueous [^{18}F]fluoride (~ 3.0 Ci; 111 GBq) was dried by iterative cycles of addition/evaporation of acetonitrile in the presence of potassium carbonate and Kryptofix 2.2.2 to form the complexation mixture of [^{18}F]K$^+$-K$_{2.2.2}$/K$_2$CO$_3$. This complex was then reacted with 2-(4-(7-butyl-3-(2-(diethylamino)-2-oxoethyl)-5-methylpyrazolo[1,5-*a*]pyrimidin-2-yl)phenoxy)ethyl 4-methylbenzenesulfonate (4.0 mg) (**4A**) at 99 °C for 20 min in anhydrous dimethyl sulfoxide (0.6 ml). [^{18}F]VUIIS1018A was purified using RP-HPLC (C18, Dynamax 250×21.4 mm; Varian), eluting with 10 mM NaH$_2$PO$_4$ buffer (pH 6.7) and ethanol (47.5/52.5, *v*/v) at 6.0 ml/min. The product was collected directly into 140 ml of water (deionized), passed through a C-18 Sep-Pak Plus (Waters, Milford, MA, USA), and eluted with 200 proof ethanol (1.0 ml) then saline (9.0 ml) into a sterile vial. Radiochemical purities were greater than 90 % in all cases and the typical specific activities were 4203 Ci/mmol (156 TBq/mmol) or greater.

Animals

All studies involving animals were conducted in compliance with federal and institutional guidelines. For glioma studies, healthy male Wistar rats were stereotactically inculcated in the right hemisphere with 1.0×10^5 C6 glioma cells (American Type Culture Collection, Manassas, VA, USA) 2 weeks prior to imaging. Rats were affixed with venous and arterial catheters prior to the MRI and PET/CT study.

MRI

PET was co-registered with MRI for anatomical comparison. In this study, rats were secured prone in a radiofrequency coil (38-mm inner diameter) and placed in a 4.7T MRI imaging system (Varian Inc., Palo Alto, CA, USA). Body temperature was maintained at 37 °C using heated airflow. In order to properly position the rats for subsequent scans, a multi-slice gradient-echo sequence (repetition time, 150 ms; echo time, 3.5 ms; matrix, 128×128; field of view, 40×40 mm^2; slice thickness, 2 mm) was employed to acquire seven slices in each

imaging plane (axial, coronal, and sagittal direction). Following this, MRI imaging was performed using a T_2-weighted fast spin-echo scan with 8 echoes and 8-ms echo spacing (effective echo time, 32 ms). The 8 coronal slices of 2 mm thickness (16 acquisitions) were collected using a repetition time of 2000 ms; field of view 32×32 mm^2 and a matrix of 128×128.

PET and CT Acquisition

In rats with confirmed tumors, PET and CT were performed within 24 h of MRI. Rats were administered [18F]VUIIS1018A *via* jugular catheter while in a microPET Focus 220 scanner (Siemens, Knoxville, TN, USA). Data were collected in listmode format for 60 or 90 min, followed by CT (microCAT II; Siemens) for attenuation correction. The dynamic PET acquisition was divided into 32 frames (12 frames (10 s per frame) for the first 2 min, 3 frames (1 min per frame) for the following 3 min, and 17 frames (5 min per frame) for the remainder of the scan). Within each frame, the raw data were binned into 3D sinograms with a span of three and ring difference of 47. The scatter and attenuation corrections were applied. The tomographic images ($128 \times 128 \times 95$) with voxel sizes of $0.095 \times 0.095 \times 0.08$ cm^3 were obtained by reconstructing the sinograms using a two-dimensional ordered-subsets expectation-maximization algorithm with 16 subsets and 4 iterations. Attenuation correction was accomplished by generating an attenuation map from the CT images. The CT images were first co-registered with PET, then segmented and projected into sinogram space with a span of 47 and ring difference of 23. Three-dimensional volumes of interest were drawn over tumor and contralateral brain using ASIPro (Siemens) in order to generate time-activity curves (TACs).

In vivo Uptake, Blocking, and Displacement of [18F]VUIIS1018A in C6 Glioma-Bearing Rats

In vivo uptake ($n = 7$), blocking ($n = 3$), and displacement studies ($n = 3$) were carried out in glioma-bearing rats. Rats were administered 1.1 ± 0.3 mCi (40.9 ± 10.1 MBq, mean $\pm$ SD) of [18F]VUIIS1018A for PET imaging. For blocking studies, [19F]VUIIS1018A (10 mg/kg) was injected 5 min [18F]VUIIS1018A administration prior to [18F]VUIIS1018A administration and initiation of a 60-min dynamic PET scan. For displacement studies, [19F]VUIIS1018A (10 mg/kg) was injected 30 min following [18F]VUIIS1018A administration during a 60-min dynamic PET scan. Regions of interest (ROIs) were selected for tumor and brain using ASIPro (Siemens).

TLC Radiometabolite Analysis

Plasma metabolites of [18F]VUIIS1018A were evaluated by thin layer chromatography (TLC). Arterial blood (200 μl) was collected at 2, 12, 30, 60, and 90 min following administration of [18F]VUIIS1018A in rats. Following centrifugation, plasma was extracted with a mixture of acetonitrile/water (340 μl, 7/1 *v/v*). The mixture was again centrifuged and the supernatant spotted on silica/glass TLC plates (Waterman, GE healthcare, USA). TLC plates were scanned using an AR-2000 radio-TLC imaging scanner (Bioscan, France) according to published methods [25].

Image Analysis and Modeling

For PET imaging analysis, TACs were generated by manually drawing three-dimensional volumes of interest over contralateral brain and tumor using ASIPro (Siemens). The arterial input function (AIF) was generated from plasma sampling (15 μl) during the dynamic imaging and corrected for metabolism of the parent ligand. For the following analysis, a two-tissue, four-rate-constant kinetic model was explored using PMOD (PMOD technologies LLC, Zurich) (Fig. 4). In this model, C_p represents the concentration of [^{18}F]VUIIS1018A in the plasma. C_t represents non-specific and free tracer in the tissue. C_m represents the specific binding of the tracer to TSPO in the outer-mitochondria membrane. The four parameters of K_1, k_2, k_3, and k_4 reflect the transport or binding rates of the tracer. In this specific study, K_1 indicates the perfusion rate of the probe from plasma to tissue (ml/min/g), while k_2 reflects the clearance rate for the tracer from tissue to plasma (1/min). k_3 and k_4 represent the specific binding rates and dissociation rates of the tracer (1/min), respectively.

Calculation of the total distribution volume (V_T) was performed based on the estimated kinetic parameters of K_1, k_2, k_3, and k_4 for different tissues. Normally, V_T is regarded as the sum of specific (V_S) and non-specific distribution (V_{ND}) (Eqs. 1, 2, and 3).

$$Vs = \frac{K_1 \cdot k_3}{k_2 \cdot k_4} \tag{1}$$

$$V_{\mathrm{ND}} = \frac{K_1}{k_2} \tag{2}$$

$$V_T = V_{\mathrm{ND}} + V_S = \frac{K_1}{k_2}\left(1 + \frac{k_3}{k_4}\right) \tag{3}$$

The binding potential (BPND) can be characterized as:

$$\mathrm{BP}_{\mathrm{ND}} = \frac{V_s}{V_{\mathrm{ND}}} = \frac{k_3}{k_4} \tag{4}$$

For receptor binding:

$$\mathrm{BP}_{\mathrm{ND}} = \frac{k_3}{k_4} = \frac{B_{\mathrm{max}}}{K_d} \tag{5}$$

where B_{max} is the concentration of the receptor in the tissue, while K_d is the equilibrium dissociation constant, which represents the concentration of radioligand occupying half of the maximum receptor population.

Calculation of the BP_{ND} parameter map was done using the Simplified Reference Tissue Model 2 (SRTM2) method [26] in the PMOD software package for the normal 60-min dynamic PET scan with [^{18}F]VUIIS1018A and for the 60-min dynamic PET scan in the blocking study with [^{19}F]VUIIS1018A administered prior to [^{18}F]VUIIS1018A. The normal cerebrum is selected as the TSPO-devoid tissue, and the tumor was selected as the TSPO-rich tissue for this analysis.

Results

SARs and Binding Affinity

The TSPO affinities of a series of pyrazolopyrimidine probes, including DPA-714, VUIIS1008, VUIIS1018A, and VUIIS1018B were analyzed by performing competitive binding assays against the isoquinoline carboxamide [^{3}H]PK 11195, a well-known TSPO ligand, in C6 glioma cell lysates (Fig. 1). Strikingly, the new probe VUIIS1018A exhibits an exceptional TSPO binding affinity (IC_{50} = 16.2 pM), which is almost 700-fold higher than DPA-714 (IC_{50} = 10.9 nM) and 20-fold higher than VUIIS1008 (IC_{50} = 0.3 nM). More interestingly, VUIIS1018B, the regioisomer of VUIIS1018A, featured an IC_{50} value of 0.1 μM, which is 6000-fold lower than VUIIS1018A. The significant difference in binding affinity indicated that modification of the 5-position of the pyrazolopyrimidine ring with a bulky n-butyl group can decrease the binding affinity dramatically, while the same modification on the 7-position leads to elevated binding affinity as compared to the parent compounds DPA-714 and VUIIS1008.

[^{18}F]VUIIS1018A Accumulation in Glioma-Bearing Rats

Accumulation of [^{18}F]VUIIS1018A was evaluated in C6 glioma-bearing rats. Uptake ($n = 7$) of [^{18}F]VUIIS1018A was evaluated using 60-min dynamic PET scans (Fig. 2). Similar to what was observed in earlier studies [23], the C6 glioma can be detected with [^{18}F]VUIIS1018A PET imaging (Fig. 2b, c) and the anatomic location of the PET signal corresponded to the tumor location as seen with T_2-weighted MRI (Fig. 2a). [^{18}F]VUIIS1018A exhibited robust accumulation in C6 gliomas with negligible accumulation observed in normal brain (Fig. 2c, d). This result is consistent with the elevated levels of TSPO in this model compared with surrounding, non-tumor brain as demonstrated through TSPO immunohistochemistry (IHC) [17–19, 23, 25, 27] and autoradiography [28, 29] in previous studies. As shown in the time-activity curves (TACs), rapid delivery of the tracer to both tumor and normal brain can be observed right after the tracer injection (Fig. 2e). [^{18}F]VUIIS1018A cleared very rapidly and did not accumulate to an appreciable extent in normal brain. In contrast, [^{18}F]VUIIS1018A rapidly accumulated in tumor tissue and increased modestly over time. Ultimately, a tumor-to-background ratio of 3:1 was achieved at the end of the 60-min scan (Fig. 2e).

Binding Specificity and Reversibility in Tumor

To further evaluate the specificity of tracer accumulation, a blocking study ($n = 3$) was conducted by administering cold [^{19}F]VUIIS1018A 5 min prior to the injection of [^{18}F]VUIIS1018A and initiation of the dynamic PET study (Fig. 3a, b). A blocking dose of 10 mg/kg [^{19}F]VUIIS1018A led to significantly elevated circulating plasma radioactivity

compared with the unblocked scenario (Fig. 3c). Furthermore, uptake of [^{18}F]VUIIS1018A in tumor tissue was significantly reduced in the blocking study. An overall reduction in tumor PET signal of 48.3 ± 2.8 % (mean ± SD, $n = 3$) was achieved with the injection of cold compound (Fig. 3c). However, the blocking dose had an insignificant effect on [^{18}F]VUIIS1018A accumulation in the normal brain.

To evaluate the reversibility of [^{18}F]VUIIS1018A accumulation in tumor and normal brain, a displacement study was conducted where cold [^{19}F]VUIIS1018A was administered 30 min following [^{18}F]VUIIS1018A administration during a dynamic PET study. Typical uptake characteristics of [^{18}F]VUIIS1018A were observed before injection of [^{19}F]VUIIS1018A in the first 30 min of the PET scan (0–30 min) (Fig. 3d). However, significant displacement of [^{18}F]VUIIS1018A in tumor tissue was observed in the final 30 min of the dynamic PET scan (30–60 min) (Fig. 3e). Accordingly, analysis of the time-activity curves (TACs) from this displacement study indicated that after the injection of [^{19}F]VUIIS1018A, the radioactivity of the tumor was reduced approximately 62.0 ± 8.0 % (mean ± SD, $n = 3$), compared with the tumor uptake in the PET analysis without displacement (Fig. 3f).

Compartmental Modeling

Pharmacokinetic modeling was used to more closely examine the uptake and clearance characteristics of [^{18}F]VUIIS1018A in tumor and normal brain. As with other TSPO PET ligands that we have evaluated in this setting [17, 18], the pharmacokinetics of [^{18}F]VUIIS1018A more closely fit a 2-tissue, 4-rate constant kinetic model in both tumor and normal brain (Fig. 4). K_1 and k_2, terms reflecting delivery and efflux from a non-binding compartment, respectively, were similar for [^{18}F]VUIIS1018A in normal brain and tumor tissue, both sharing a smaller K_1 when compared with k_2. Meanwhile, both tumor and brain have a higher specific binding rate (k_3) when compared with the dissociation rate (k_4) (Suppl. Table 1, ESM). The most notable difference in tracer pharmacokinetics between tumor and normal brain was observed in k_3/k_4, or the parameter describing binding potential BPND. The tumor features an 8-fold higher k_3/k_4 when compared with k_3/k_4 of healthy brain (Table 1). According to Eq. 5, these data are in agreement with the higher TSPO expression level in brain tumors relative to normal brain. Parametric images were constructed to compare the binding potential BP$_{ND}$ of [^{18}F]VUIIS1018A with and without blocking by [^{19}F]VUIIS1018A (Fig. 5). As shown in Fig. 5b, d, blocking significantly lowers BP$_{ND}$ in the glioma tumor.

Comparison of Pharmacokinetics of [^{18}F]VUIIS1018A, [^{18}F]DPA-714, and [^{18}F]VUIIS1008

The *in vivo* performance of [^{18}F]VUIIS1018A compared favorably to two other TSPO PET agents we previously evaluated in this setting, [^{18}F]DPA-714 and [^{18}F]VUIIS1008. In both healthy brain and tumor tissue, [^{18}F]VUIIS1018A exhibited a lower influx-to-efflux parameter ($K1/k2$) when compared with [^{18}F]DPA-714 and [^{18}F]VUIIS1008 (Table 1). In normal brain, [^{18}F]VUIIS1018A features a lower k_3/k_4 when compared with [^{18}F]DPA-714 (2.91 *vs.* 4.02) and [^{18}F]VUIIS1008 (2.91 *vs.* 4.43) (Table 1), suggesting a lower binding potential (BP$_{ND}$) and binding preference in healthy brain. However, the opposite trend was observed in tumor tissue, where the value for BP$_{ND}$ (k_3/k_4) was higher for [^{18}F]VUIIS1018A compared to [^{18}F]DPA-714 (23.10 *vs.* 8.91) [17] and [^{18}F]VUIIS1008

(23.10 *vs.* 12.63) [25] (Table 1), indicating a higher binding potential (BP_{ND}) and binding preference in tumor. Taken together, these results appear to be congruent with the relative affinities of these probes (Fig. 1) and suggest potentially higher tumor avidity and lower brain avidity of our new tracer.

Furthermore, although calculated V_T for tumor and normal brain were higher for [18F]DPA-714 and [18F]VUIIS1008, V_T ratios between tumor and normal brain were higher for [18F]VUIIS1018A when compared with [18F]DPA-714 (9.1 *vs.* 4.4) and [18F]VUIIS1008 (9.1 *vs.* 6.0), which led to the improved signal-to-noise ratio and imaging contrast with this tracer.

Discussion

In our previous studies, we reported the utilization of several probes for quantitative PET imaging of TSPO expression in preclinical glioma studies. These probes include [18F]PBR06 [18], [18F]DPA-714 [17] and [18F]VUIIS1008 [23, 25]. In these studies, the TSPO probes displayed significant capability for discriminating the tumors from the surrounding normal brain. More importantly, using compartmental analysis, the TSPO levels could be quantitatively assayed in tumors [17, 18, 25]. However, potential drawbacks associated with these prior radiotracers included (1) tracer accumulation in the normal brain which reached a sufficient level to prevent the detection of gliomas with modest TSPO expression, such as lower grade disease and (2) significant metabolism *in vivo*, which required further AIF correction for the following quantitative analysis. While demonstrating the potential of TSPO PET to detect gliomas, these studies motivated us to develop novel TSPO PET tracers with improved profiles for cancer imaging.

Herein, we quantitatively evaluated the *in vivo* performance of a novel TSPO probe [18F]VUIIS1018A in preclinical glioma imaging studies. [18F]VUIIS1018A was synthesized by modifying the 7-position of the pyrazolopyrimidine ring with an n-butyl group instead of the 7-methyl group found on [18F]DPA-714 (Suppl. Scheme 1 and Fig. 1). This resulted in a TSPO-probe with approximately 700-fold greater TSPO affinity when compared with [18F]DPA-714 [17, 23]. Furthermore, as illustrated in this study, this optimization also resulted in a variety of intriguing and improved properties for cancer imaging. For example, [18F]VUIIS1018A exhibits significantly lower accumulation in healthy brain, as illustrated by the TACs, V_T and brain binding potential BP_{ND}, when compared to previously reported TSPO probes. This could prove advantageous when attempting to discriminate lower grade gliomas, which have low TSPO expression, from the healthy brain. More practically compared to the parent tra cer s [18F]DP A-71 4 a nd [18F]VUIIS100 8, [18F]VUIIS1018A exhibited an improved tumor-to-background ratio, a higher specific-to-non-specific binding ratio and a higher tumor binding potential, which made the new tracer a better candidate for detecting tumors with modest TSPO expression profiles.

Conclusion

In this study, we developed a novel TSPO PET tracer [18 F]VUIIS1018A by replacing the 7-methyl group on the pyrazolopyrimidine ring of DPA-714 with an n-butyl group. The new

tracer exhibited an exceptional binding affinity to TSPO with an IC_{50} value of 16.2 pM, which is a 700-fold improvement compared with DPA-714. Taking advantage of this tracer's significantly lower accumulation in healthy brain and higher tumor binding potential, the new tracer can serve as a better candidate to image low grade tumors or tumors with modest TSPO expression. We envision that [^{18}F]VUIIS1018A can be a very promising PET ligand for glioma diagnostics, and could possibly be used in other TSPO related diseases.

Supplementary Material

Refer to Web version on PubMed Central for supplementary material.

Acknowledgements.

References

1. Dhermain FG, Hau P, Lanfermann H, Jacobs AH, van den Bent MJ (2010) Advanced MRI and PET imaging for assessment of treatment response in patients with gliomas. Lancet Neurol 9:906–920 [PubMed: 20705518]

2. Dimitrakopoulou-Strauss A, Seiz M, Tuettenberg J, Schmieder K, Eisenhut M, Haberkorn U, Strauss LG (2011) Pharmacokinetic studies of ^{68}Ga-labeled Bombesin (^{68}?Ga-BZH3) and F-^{18}FDG PET in patients with recurrent gliomas and comparison to grading: preliminary results. Clin Nucl Med 36:101–108 [PubMed: 21220970]

3. Papadopoulos V, Baraldi M, Guilarte TR, Knudsen TB, Lacapère JJ, Lindemann P, Norenberg MD, Nutt D, Weizman A, Zhang MR, Gavish M (2006) Translocator protein (18kDa): new nomenclature for the peripheral-type benzodiazepine receptor based on its structure and molecular function. Trends Pharmacol Sci 27:402–409 [PubMed: 16822554]

4. Chauveau F, Boutin H, Van Camp N et al. (2008) Nuclear imaging of neuroinflammation: a comprehensive review of [^{11}?C]PK11195 challengers. Eur J Nucl Med Mol Imaging 35:2304–2319 [PubMed: 18828015]

5. Doorduin J, de Vries EF, Dierckx RA, Klein HC (2008) PET imaging of the peripheral benzodiazepine receptor: monitoring disease progression and therapy response in neurodegenerative disorders. Curr Pharm Des 14:3297–3315 [PubMed: 19075709]

6. Venneti S, Lopresti BJ, Wiley CA (2006) The peripheral benzodiazepine receptor (translocator protein 18kDa) in microglia: from pathology to imaging. Prog Neurobiol 80:308–322 [PubMed: 17156911]

7. Maeda J, Higuchi M, Inaji M, Ji B, Haneda E, Okauchi T, Zhang MR, Suzuki K, Suhara T (2007) Phase-dependent roles of reactive microglia and astrocytes in nervous system injury as delineated by imaging of peripheral benzodiazepine receptor. Brain Res 1157:100–111 [PubMed: 17540348]

8. Rupprecht R, Papadopoulos V, Rammes G, Baghai TC, Fan J, Akula N, Groyer G, Adams D, Schumacher M (2010) Translocator protein (18 kDa) (TSPO) as a therapeutic target for neurological and psychiatric disorders. Nat Rev Drug Discov 9:971–988 [PubMed: 21119734]

9. Han Z, Slack RS, Li W, Papadopoulos V (2003) Expression of peripheral benzodiazepine receptor (PBR) in human tumors: relationship to breast, colorectal, and prostate tumor progression. J Recept Signal Transduct Res 23:225–238 [PubMed: 14626449]

10. Hardwick M, Fertikh D, Culty M, Li H, Vidic B, Papadopoulos V (1999) Peripheral-type benzodiazepine receptor (PBR) in human breast cancer: correlation of breast cancer cell aggressive

phenotype with PBR expression, nuclear localization, and PBR-mediated cell proliferation and nuclear transport of cholesterol. Cancer Res 59:831–842 [PubMed: 10029072]

11. Hardwick M, Rone J, Han Z, Haddad B, Papadopoulos V (2001) Peripheral-type benzodiazepine receptor levels correlate with the ability of human breast cancer MDA-MB-231 cell line to grow in SCID mice. Int J Cancer 94:322–327 [PubMed: 11745409]

12. Corsi L, Geminiani E, Baraldi M (2008) Peripheral benzodiazepine receptor (PBR) new insight in cell proliferation and cell differentiation review. Curr Clin Pharmacol 3:38–45 [PubMed: 18690876]

13. Deane NG, Manning HC, Foutch AC, Washington MK, Aronow BA, Bornhop DJ, Coffey RJ (2007) Targeted imaging of colonic tumors in smad3–/– mice discriminates cancer and inflammation. Mol Cancer Res 5:341–349 [PubMed: 17426249]

14. Wyatt SK, Manning HC, Bai M, Bailey SN, Gallant P, Ma G, McIntosh L, Bornhop DJ (2010) Molecular imaging of the translocator protein (TSPO) in a pre-clinical model of breast cancer. Mol Imaging Biol 12:349–358 [PubMed: 19949989]

15. Vasdev N, Green DE, Vines DC, McLarty K, McCormick PN, Moran MD, Houle S, Wilson AA, Reilly RM (2013) Positron-emission tomography imaging of the TSPO with [^{18}?F]FEPPA in a preclinical breast cancer model. Cancer Biother Radiopharm 28:254–259 [PubMed: 23350894]

16. Zheng J, Boisgard R, Siquier-Pernet K, Decaudin D, Dollé F, Tavitian B (2011) Differential expression of the 18 kDa translocator protein (TSPO) by neoplastic and inflammatory cells in mouse tumors of breast cancer. Mol Pharm 8:823–832 [PubMed: 21417480]

17. Tang D, Hight MR, McKinley ET et al. (2012) Quantitative preclinical imaging of TSPO expression in glioma using N,N-diethyl-2-(2-(4-(2-^{18}?F-fluoroethoxy)phenyl)-5,7-dimethylpyrazolo[1,5-a]pyrimidin-3-yl)acetamide. J Nucl Med 53:287–294 [PubMed: 22251555]

18. Buck JR, McKinley ET, Hight MR et al. (2011) Quantitative, preclinical PET of translocator protein expression in glioma using ^{18}F-N-fluoroacetyl-N-(2,5-dimethoxybenzyl)-2-phenoxyaniline. J Nucl Med 52:107–114 [PubMed: 21149488]

19. Cheung YY, Nickels ML, Tang D, Buck JR, Manning HC (2014) Facile synthesis of SSR180575 and discovery of 7-chloro-N,N,5-trimethyl-4-oxo-3(6-[^{18}?F]fluoropyridin-2-yl)-3,5-dihydro-4H-pyri dazino[4,5-b]in-dole-1-acetamide, a potent pyridazinoindole ligand for PET imaging of TSPO in cancer. Bioorg Med Chem Lett 24:4466–4471 [PubMed: 25172419]

20. Buck JR, McKinley ET, Fu A et al. (2015) Preclinical TSPO ligand PET to visualize human glioma xenotransplants: a preliminary study. PLOS One 10:e0141659

21. Winkeler A, Boisgard R, Awde AR, Dubois A, Thézé B, Zheng J, Ciobanu L, Dollé F, Viel T, Jacobs AH, Tavitian B (2012) The translocator protein ligand [^{18}?F]DPA-714 images glioma and activated microglia in vivo. Eur J Nucl Med Mol Imaging 39:811–823 [PubMed: 22270507]

22. Venneti S, Lopresti BJ, Wiley CA (2013) Molecular imaging of microglia/macrophages in the brain. Glia 61:10–23 [PubMed: 22615180]

23. Tang D, McKinley ET, Hight MR et al. (2013) Synthesis and structure-activity relationships of 5,6,7-substituted pyrazolopyrimidines: discovery of a novel TSPO PET ligand for cancer imaging. J Med Chem 56:3429–3433 [PubMed: 23521048]

24. Tang D, Buck JR, Hight MR, Manning HC (2010) Microwave-assisted organic synthesis of a high-affinity pyrazolo-pyrimidinyl TSPO ligand. Tetrahedron Lett 51:4595–4598 [PubMed: 20689673]

25. Tang D, Nickels ML, Tantawy MN, Buck JR, Manning HC (2014) Preclinical imaging evaluation of novel TSPO-PET ligand 2-(5,7-Diethyl-2-(4-(2-[^{18}?F]fluoroethoxy)phenyl)pyrazolo[1,5-a]pyrimidin-3-yl)-N,N-diethylacetamide ([18?F]VUIIS1008) in glioma. Mol Imaging Biol 16:813–820 [PubMed: 24845529]

26. Wu Y, Carson RE (2002) Noise reduction in the simplified reference tissue model for neuroreceptor functional imaging. J Cereb Blood Flow Metab 22:1440–1452 [PubMed: 12468889]

27. Tang D, Li J, Buck JR, Tantawy MN, Xia Y, Harp JM, Nickels ML, Meiler J, Manning HC (2017) Evaluation of TSPO PET ligands [^{18}?F]VUIIS1009A and [^{18}?F]VUIIS1009B: tracers for cancer imaging. Mol Imaging Biol 19:578–588 [PubMed: 27853987]

28. Starosta-Rubinstein S, Ciliax BJ, Penney JB, McKeever P, Young AB (1987) Imaging of a glioma using peripheral benzodiazepine receptor ligands. Proc Natl Acad Sci U S A 84:891–895 [PubMed: 3027710]

29. Black KL, Ikezaki K, Toga AW (1989) Imaging of brain tumors using peripheral benzodiazepine receptor ligands. J Neurosurg 71:113–118 [PubMed: 2544689]
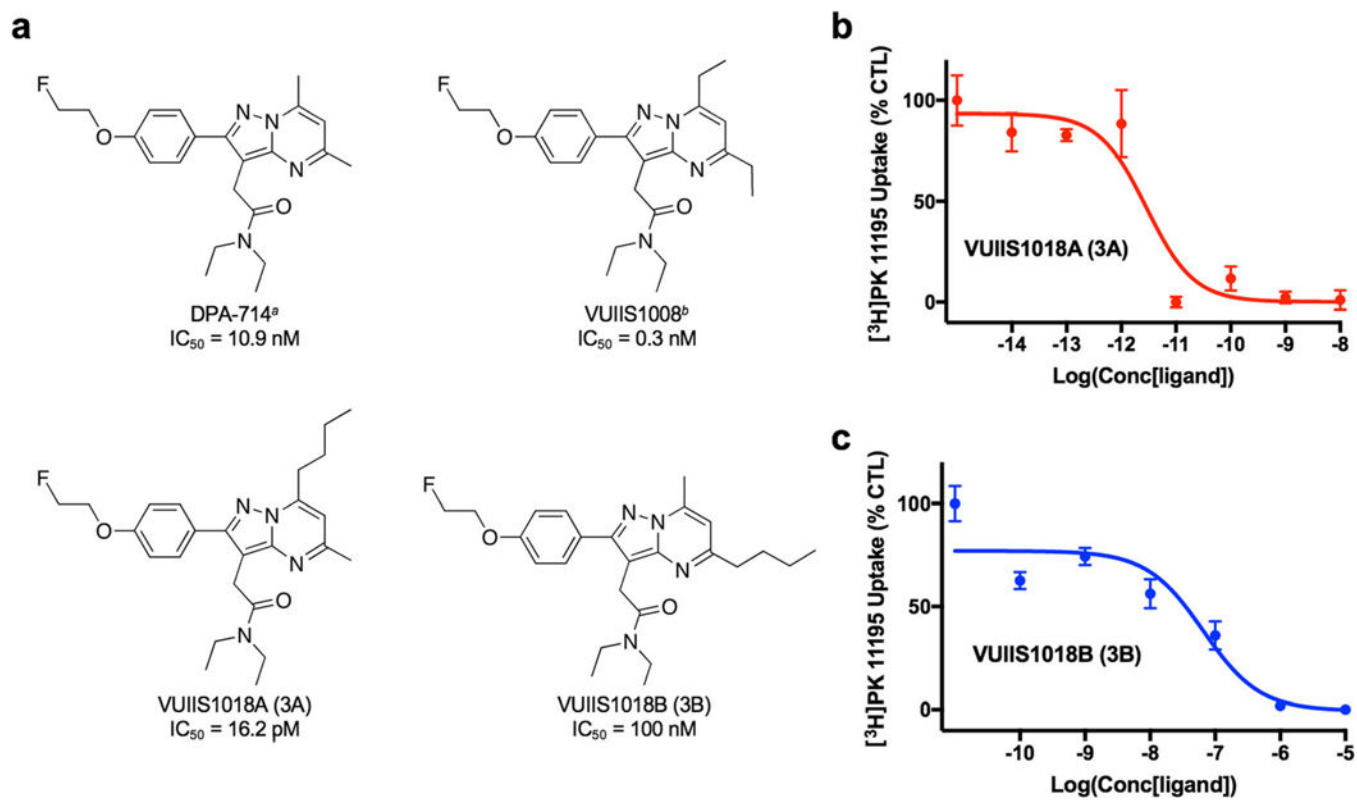
Fig. 1.
a Chemical structure and IC$_{50}$ values of DPA-714 ([a]see ref. [17]), VUIIS1008 ([b]see ref. [23]), VUIIS1018A, and VUIIS1018B. Equilibrium competitive binding of [^{3}H]PK 11195 using **b** VUIIS1018A and **c** VUIIS1018B in C6 glioma cell lysate.
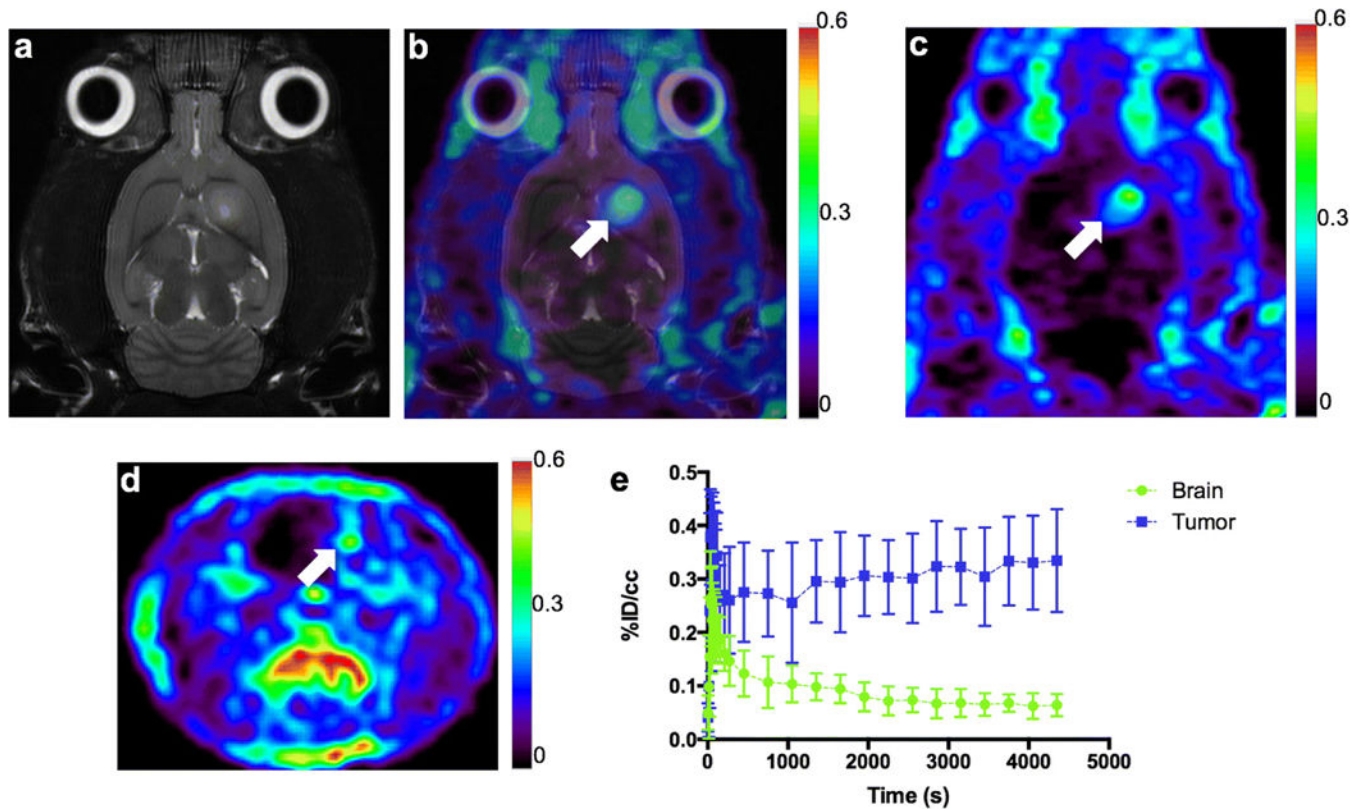
Fig. 2.
a T$_2$-weighted MR image (coronal) of a C6 glioma-bearing rat. b Co-registration of [^{18}F]VUIIS1018A PET image with the T$_2$-weighted MR image for the same C6 glioma-bearing rat. **c** Coronal PET image of the same C6 glioma-bearing rat obtained from dynamic scan with [^{18}F]VUIIS1018A. **d** Transverse PET image of the same C6 glioma-bearing rat obtained from dynamic scan with [^{18}F]VUIIS1018A. **e** Time activity curves (TACs) for the tumor (blue) and contralateral brain (green) in the 60-min dynamic scan ($n = 7$). %ID/cm^3 = percentage injected dose per cubic centimeter. In TACs, data = mean ± SD. Tumor is marked by the white arrow on the image.
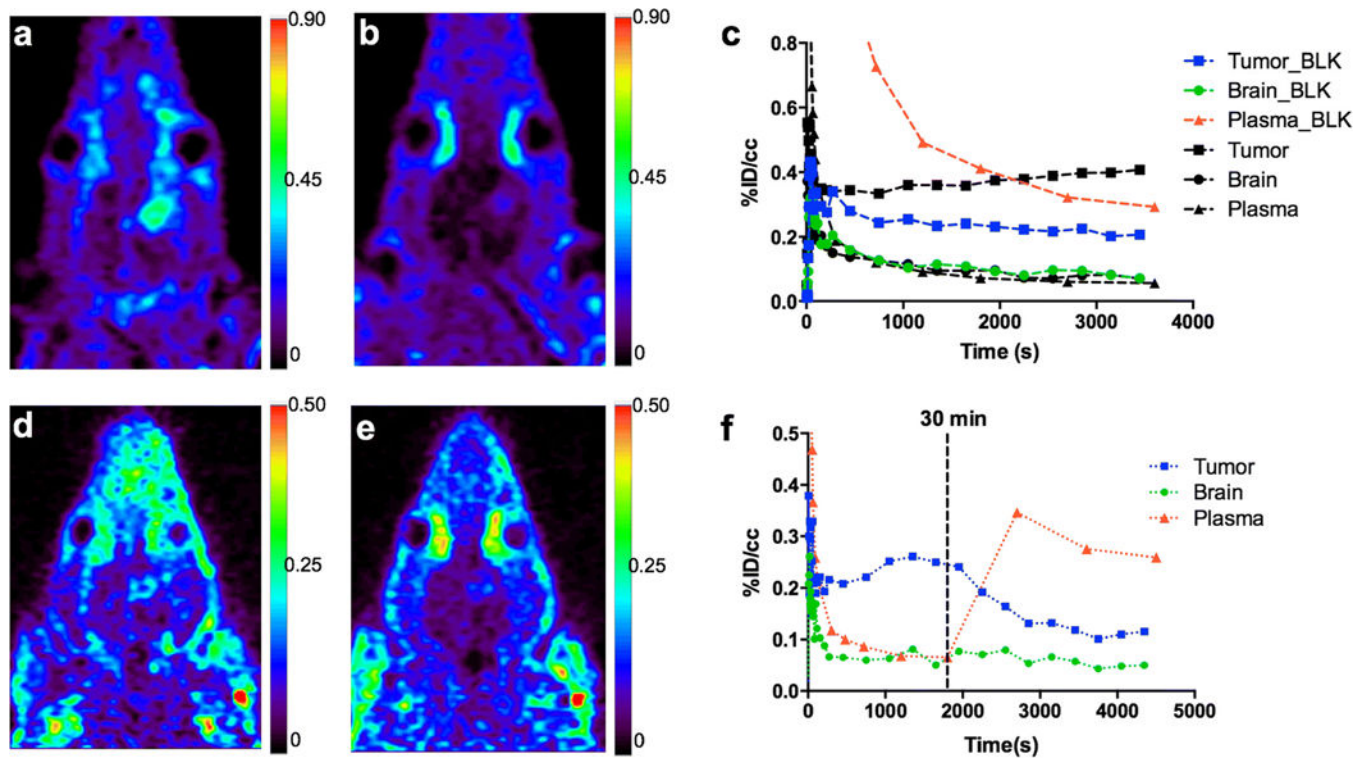
Fig. 3.
Blocking study with administration of [^{19}F]VUIIS1018A (10 mg/kg) 5 min before administration of [^{18}F]VUIIS1018A and a 60-min dynamic PET scan. **a** Coronal PET image of C6 glioma-bearing rat obtained from dynamic scan with [^{18}F]VUIIS1018A (no blockade). **b** Uptake characteristics of [^{18}F]VUIIS1018A following pre-blocking with [^{19}F]VUIIS1018A (10 mg/kg) in the same rat (coronal view). **c** Representative TACs for tumor (black and blue squares), contralateral brain (black and green circles), and plasma (black and red triangles) in the normal (un-blocked) 60-min dynamic (black) and pre-blocked 60-min dynamic (blue, green, and red) PET scans in the same rat. Chase study with administration of [^{19}F]VUIIS1018A (10 mg/kg) at 30 min during a 60-min dynamic PET scan. **d** Summation of the first 30 min of a 60-min dynamic PET acquisition following administration of [^{18}F]VUIIS1018A, prior to injection of [^{19}F]VUIIS1018A. **e** Summation of the last 30 min of the dynamic acquisition following administration of [^{18}F]VUIIS1018A after injection of [^{19}F]VUIIS1018A. **f** Representative TACs for tumor (blue), contralateral brain (green), and plasma (red) in the displacement assay. %ID/cm^3 = percentage injected dose per cubic centimeter.
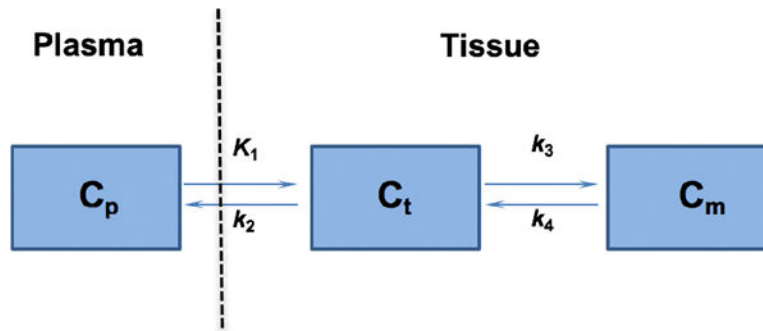
Fig. 4.
The 2-tissue, 4-kinetic-parameter model used for describing [^{18}F]VUIIS1018A kinetics in reference tissues, including tumor and brain. In this model, C_p represents the concentration of [^{18}F]VUIIS1018A in the plasma. C_t represents non-specific and free tracer in the tissue. C_m represents the specific binding of the tracer to TSPO in the outer-mitochondria membrane. The four parameters of K_1, k_2, k_3, and k_4 reflect the transport or binding rates of the tracer. In this specific study, K_1 indicates the perfusion rate of the probe from plasma to tissue, while k_2 reflects the clearance rate for the tracer from tissue to plasma. k_3 and k_4 represent the specific binding rates and dissociation rates of the tracer, respectively.
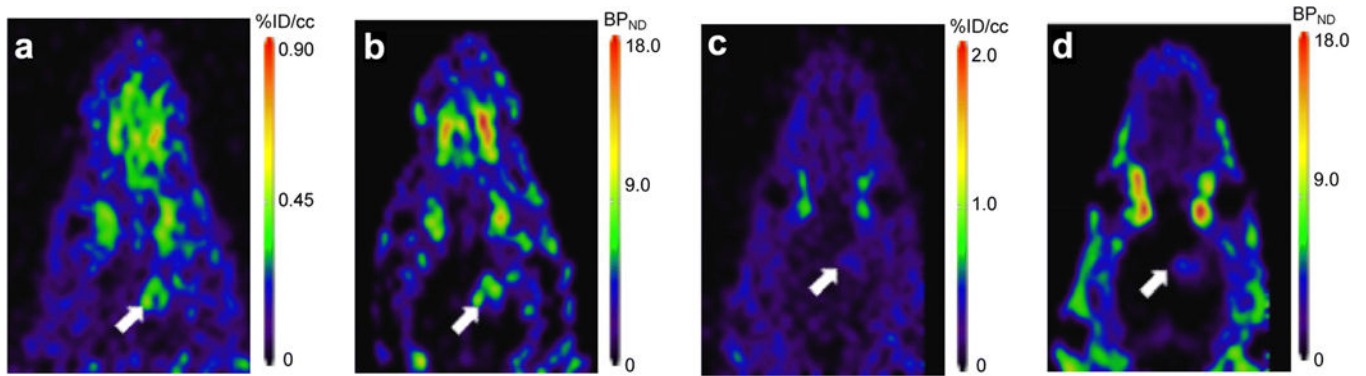
Fig. 5.
Sixty-minute dynamic PET scans of [^{18}F]VUIIS1018A were obtained with and without blocking by [^{19}F]VUIIS1018A. The blocking study was performed with administration of [^{19}F]VUIIS1018A (10 mg/kg) 5 min before administration of [^{18}F]VUIIS1018A and a 60-min dynamic PET scan. Binding potential BP_{ND} was calculated for both of these images. **a** Distribution of [^{18}F]VUIIS1018A in the 60-min dynamic PET scan. **b** Calculated BP_{ND} parameter map for the 60-min dynamic PET scan. **c** Imaging for the 60-min dynamic PET scan in the blocking study. **d** Calculated BP_{ND} parameter map for the blocking study. Arrows indicate tumors.

Table 1.

Pharmacokinetic parameters obtained from analysis using the two-tissue, 4-rate constant kinetic model (Fig. 4) for [^{18}F]DPA-714^{a,b} ($n = 11$), [^{18}F]VUIIS1008^{b} ($n = 5$), and [^{18}F]VUIIS1018A ($n = 7$). Results = mean $\pm$ SEM

Probe	Region	K_1/k_2	k_3/k_4	V_T
[^{18}F]DPA-714^{a,b}	Tumor	6.867 ± 1.226	8.913 ± 1.155	70.033 ± 14.729
	Brain	3.619 ± 0.551	4.024 ± 0.842	15.963 ± 3.566
[^{18}F]VUIIS1008^{b}	Tumor	1.902 ± 0.816	12.634 ± 1.406	25.224 ± 10.035
	Brain	0.855 ± 0.325	4.435 ± 1.387	4.210 ± 1.612
[^{18}F]VUIIS1018A	Tumor	0.532 ± 0.130	23.097 ± 4.757	11.036 ± 3.731
	Brain	0.311 ± 0.036	2.913 ± 0.456	1.214 ± 0.190

[a] See ref. [17]

[b] See ref. [25]